

# The reduced classical car-following model: stability analyses and design guidelines

Gopal Krishna Kamath, Krishna Jagannathan and Gaurav Raina Department of Electrical Engineering,  
Indian Institute of Technology Madras, Chennai 600 036, India  
Email: {ee12d033, krishnaj, gaurav}@ee.iitm.ac.in

## Abstract

Reaction delays play an important role in determining the qualitative dynamical properties of a platoon of vehicles driving on a straight road. In this paper, we investigate the impact of delayed feedback on the dynamics of a recently-proposed car-following model; namely, the Reduced Classical Car-Following Model (RCCFM). Specifically, we analyse the RCCFM in three regimes – no delay, small delay and arbitrary delay. The control-theoretic analyses for no-delay and small-delay regimes yield a sufficient condition for local stability of the RCCFM. Next, we derive the necessary and sufficient condition for local stability of the RCCFM for an arbitrary delay. We then demonstrate that the transition of traffic flow from the locally stable to the unstable regime occurs via a Hopf bifurcation.

In the context of self-driven vehicles, designing control algorithms that avoid jerky vehicular movements is essential. Hence, we derive the necessary and sufficient condition for non-oscillatory convergence of the RCCFM, thus ensuring smooth traffic flow and good ride quality. Next, we characterise the rate of convergence of the RCCFM, and bring forth the interplay between non-oscillatory convergence and the rate of convergence of the RCCFM. Finally, we present some simulations that validate the theoretical analysis.

Qualitatively, since a Hopf bifurcation results in the emergence of limit cycles, we characterise the type of the Hopf bifurcation and the asymptotic orbital stability of the limit cycles using Poincaré normal forms and the center manifold theory. These limit cycles manifest as back-propagating congestion waves. The analysis is complemented with stability charts, bifurcation diagrams and MATLAB simulations.

## Index Terms

Transportation networks, car-following models, time delays, stability, convergence, Hopf bifurcation.

## I. INTRODUCTION

Intelligent transportation systems constitute a substantial theme of discussion on futuristic smart cities. A prospective solution to increase resource utilisation is to use self-driven vehicles, which may also mitigate traffic congestion [23, Section 5.2], [27]. To that end, it is imperative to design stable control algorithms for these vehicles. Since

A conference version of this paper appeared in Proceedings of the 53<sup>rd</sup> Annual Allerton Conference on Communication, Control and Computing, pp. 538-545, 2015. DOI: 10.1109/ALLERTON.2015.7447051

a good design process requires an in-depth understanding of vehicular dynamics, a class of dynamical models – known as car-following models – have been developed and studied [3]–[5], [8], [9], [18], [30].

An important consideration in the study of car-following models is the delay in the dynamical variables. Delays arise due to various factors such as sensing, mechanical motions, communication and signal processing. These delays are known to have a variety of effects on the properties of a dynamical system [14]. Specifically, delays can readily lead to oscillations and instability [24], [30].

In this paper, we investigate the impact of delayed feedback on the qualitative dynamical properties of a platoon of vehicles driving on a straight road. Specifically, we focus on analysing the effect of delayed feedback on the Reduced Classical Car-Following Model (RCCFM) [8]. In the specific context of human-driven vehicles, the dominant sources of delay are the physiological delay and the mechanical delay [24]. However, for self-driven vehicles, reaction delays tend to be smaller than those of human-driven vehicles, and typically occur due to the delays in sensing, computation and actuation [1]. Hence, our analysis of the RCCFM is performed in three regimes; namely, *(i)* no delay, *(ii)* small delay and *(iii)* arbitrary delay. We derive a sufficient condition for the local stability of the RCCFM for small delays, and for the arbitrary-delay regime, we analytically characterise the stable region for the RCCFM.

In addition to stability, non-oscillatory convergence and rate of convergence constitute two properties of practical interest, which we also derive for the RCCFM. Such conditions could aid in ensuring smooth traffic flow by avoiding jerky vehicular motion, thereby improving ride quality. The theoretical analyses could offer suggestions for design guidelines.

In the context of human-driven vehicles, our investigation into the impact of reaction delay enhances phenomenological insights into the emergence and evolution of traffic congestion. For example, a peculiar phenomenon known as a ‘phantom jam’ – the emergence of a back-propagating congestion wave in motorway traffic, seemingly out of nowhere – has been observed in the real world [4], [5]. Previous studies [4], [5] have shown that a change in driver’s sensitivity (for instance, a sudden deceleration) can lead to such oscillatory behaviour. In this paper, we show that similar oscillations could also result from an increase in the driver’s reaction delay. More generally, our study leads to an important observation that the transition of traffic flow from stability to instability could take place due to a variation in many combinations of model parameters. In order to capture this complex dependence on various parameters, we introduce an exogenous, non-dimensional parameter in our dynamical model, set to unity on the stability boundary. We then analyse the system behaviour as this exogenous parameter pushes the system across the stability boundary, and show that limit cycles emerge due to a certain bifurcation exhibited by the dynamical system.

The impact of the reaction delay is perhaps even more important in the context of self-driven vehicles. Self-driven vehicles are envisioned to have reduced reaction delays as compared to a human driver. As a result, self-driven vehicles facilitate smaller equilibrium separation between consecutive vehicles [23, Section 5.2]. This, in turn, improves resource utilisation without compromising safety [27]. In contrast to the case of human-driven vehicles, the parameters in the control algorithm – known as upper longitudinal control algorithm [23, Section 5.2] – for

self-driven vehicles need to be tuned appropriately. To that end, our analyses and findings highlight the quantitative impact of delayed feedback on the design of control algorithms for self-driven vehicles. In particular, the combination of stability, convergence and detailed bifurcation analyses may help in the design of various aspects of a longitudinal control algorithm [23, Section 5.2]. We corroborate our analytical findings using stability charts, bifurcation diagrams and MATLAB simulations.

#### A. Related work on car-following models

The work by Chandler *et al.* [19] as well as the one by Herman *et al.* [21] constitute two of the earliest known investigations on stability of car-following models. Some well-known models, and their modifications, have been investigated in [3], [19] and [6]. For a recent exposition of linear stability analysis as applied to car-following models, see [20]. The aforementioned investigations mainly use transform techniques to derive conditions for stability. In contrast, [30] and some of the references therein consider the issue of stability from a dynamical systems perspective. In [8], it was showed that the RCCFM undergoes a Hopf bifurcation. Therein, for the first time, the effect of the delay resulting from the velocity of the vehicle itself was accounted for.

From a vehicular dynamics perspective, most upper longitudinal controllers in the literature assume the lower controller's dynamics to be well-modeled by a first-order control system, in order to capture the delay lag [23, Section 5.3]. The upper longitudinal controllers are then designed to maintain either constant velocity, spacing or time gap; for details, see [22] and the references therein. Specifically, Rajamani *et al.* [22] prove that synchronisation with the lead vehicle is possible by using information only from the vehicle directly ahead. This reduces implementation complexity, and does not mandate vehicles to be installed with communication devices.

However, in the context of autonomous vehicles, communication systems are required to exchange various system states required for the control algorithm. This information is used either for distributed control [22] or coordinated control [31]. Formation and platoon stabilities have also been studied considering information flow among the vehicles [25], [28]. For an extensive review, see [15].

#### B. Our contributions

Our contributions are as follows.

- (1) We derive the RCCFM, and analyse it in three regimes; namely, *(i)* no delay, *(ii)* small delay and *(iii)* arbitrary delay. We prove that the ideal case of instantaneously-reacting drivers is stable for all practically significant parameter values. We then derive the stability condition for the small-delay regime using time-linearisation technique.
- (2) For the case of an arbitrary delay, it is known that the RCCFM undergoes a Hopf bifurcation [8]. We summarise the necessary and sufficient condition for the local stability of the RCCFM and highlight that it indeed generalises the results derived for no-delay and small-delay regimes. We then characterise the type of Hopf bifurcation and the asymptotic orbital stability of the emergent limit cycles using Poincaré normal forms and the center manifold theory [2].

- (3) In the case of human-driven vehicles, our work enhances phenomenological insights into the emergence and evolution of traffic congestion. For example, the Hopf bifurcation analysis provides a mathematical framework to offer a possible explanation for the observed ‘phantom jams’ [8].
- (4) We derive the necessary and sufficient condition for non-oscillatory convergence of the RCCFM. This is useful in the context of a transportation network since oscillations lead to jerky vehicular movements, thereby degrading ride quality and possibly causing collisions.
- (5) We characterise the rate of convergence of the RCCFM, thereby gaining insights into the time required for the platoon to equilibrate, when perturbed. Such perturbations occur, for instance, when a vehicle departs from a platoon.
- (6) We highlight the trade-off between non-oscillatory convergence and the rate of convergence. Considering this trade-off, we suggest some guidelines to appropriately choose parameters for the upper longitudinal control algorithm in self-driven vehicles.
- (7) We corroborate the analytical results with the aid of stability charts, numerical computations and MATLAB simulations.

The remainder of this paper is organised as follows. In Section II, we summarise the Classical Car-Following Model (CCFM) and derive the RCCFM. In Sections III, IV and V, we characterise the stable region for the RCCFM in no-delay, small-delay and arbitrary-delay regimes respectively. We understand the stable region by characterising the region of non-oscillatory convergence of the RCCFM in Section VI, and the rate of convergence of the RCCFM in Section VII. In Section VIII, we present the local Hopf bifurcation analysis for the RCCFM. In Section IX, we present the simulation results, and conclude in Section X.

## II. MODELS

We begin this section with an overview of the setting of our work. We then briefly explain the CCFM, before ending the section by deriving the RCCFM.

### A. The setting

We study a platoon of  $N + 1$  ‘ideal’ (*i.e.*, zero length) vehicles traversing an infinitely long, single-lane road without overtaking. The lead vehicle is indexed 0, its follower 1, and so forth. Each vehicle updates its acceleration based on a combination of its position, velocity and acceleration and those of the vehicle directly ahead. Let  $x_i(t)$ ,  $\dot{x}_i(t)$  and  $\ddot{x}_i(t)$  denote the position, velocity and acceleration of the  $i^{th}$  vehicle respectively, at time  $t$ . The acceleration and velocity profiles of the lead vehicle are assumed to be known. In particular, we restrict ourselves to leader profiles that converge, in finite time, to  $\ddot{x}_0 = 0$  and  $\dot{x}_0 < \infty$ ; that is, there exists a finite  $T_0$  such that  $\ddot{x}_0(t) = 0$ ,  $\dot{x}_0(t) = \dot{x}_0$ ,  $\forall t \geq T_0$ . We use the terms “driver” and “vehicle” interchangeably throughout.

### B. The Classical Car-Following Model (CCFM)

A key feature of the CCFM is that the acceleration of each vehicle is dependent on three quantities: (i) its own velocity, (ii) velocity relative to the vehicle directly ahead, and (iii) distance to the vehicle directly ahead. The exact

dependence has been modeled in the literature as [3]

$$\ddot{x}_i(t) = \alpha_i \frac{(\dot{x}_i(t))^m (\dot{x}_{i-1}(t - \tau) - \dot{x}_i(t - \tau))}{(x_{i-1}(t - \tau) - x_i(t - \tau))^l}, \quad (1)$$

for  $i \in \{1, 2, \dots, N\}$ . Here,  $\alpha_i$  represents the  $i^{\text{th}}$  driver's sensitivity coefficient and  $\alpha_i > 0$  for each  $i \in \{1, 2, \dots, N\}$ . Also,  $m \in [-2, 2]$  and  $l \in \mathbb{R}_+$  are model parameters that contribute to the non-linearity. Note that the reaction delay is neglected in the self-velocity term  $(\dot{x}_i(t))^m$ . In this paper, we account for this delay, in addition to the heterogeneity in reaction delays for different vehicles.

### C. The Reduced Classical Car-Following Model (RCCFM)

It is apparent from (1) that the state variable  $x_i(t)$  becomes unbounded as  $t \rightarrow \infty$  for each  $i$ . Therefore, similar to [30], we transform the model in (1) using  $y_i(t) + b = x_{i-1}(t) - x_i(t)$  and  $v_i(t) = \dot{y}_i(t) = \dot{x}_{i-1}(t) - \dot{x}_i(t)$  for  $i \in \{1, 2, \dots, N\}$ . Here,  $b$  denotes the desired equilibrium separation,  $y_i(t) + b$  represents the separation between vehicles  $i - 1$  and  $i$  at time  $t$ , and  $v_i(t)$  corresponds to the relative velocity of the  $i^{\text{th}}$  vehicle with respect to the  $(i - 1)^{\text{th}}$  vehicle at time  $t$ . The transformed model is thus obtained as

$$\begin{aligned} \dot{v}_i(t) &= \beta_{i-1}(t - \tau_{i-1})v_{i-1}(t - \tau_{i-1}) - \beta_i(t - \tau_i)v_i(t - \tau_i), \\ \dot{y}_i(t) &= v_i(t), \end{aligned} \quad (2)$$

for  $i \in \{1, 2, \dots, N\}$ . Here,

$$\beta_i(t) = \alpha_i \frac{(\dot{x}_0(t) - v_0(t) - \dots - v_i(t))^m}{(y_i(t - \tau) + b)^l}.$$

Note that  $y_0$ ,  $v_0$ ,  $\alpha_0$  and  $\tau_0$  are dummy variables introduced for notational brevity, all of which are set to zero. We emphasise that  $y_0$  and  $v_0$  are *not* state variables.

In the present work, we consider the case when  $l = 0$ . This restriction decouples the dynamics of  $v_i$  from that of  $y_i$  for each  $i$ . Further, we drop the state variables  $\{y_i\}_{i=1}^N$  since they correspond to the integral of the respective  $v_i$ 's, thus reducing the dimension of the state space from  $2N$  to  $N$ . This results in the Reduced Classical Car-Following Model (RCCFM) described by the following non-linear, time-delayed equation:

$$\dot{v}_i(t) = \beta_{i-1}(t - \tau_{i-1})v_{i-1}(t - \tau_{i-1}) - \beta_i(t - \tau_i)v_i(t - \tau_i), \quad (3)$$

with  $\beta_i(t) = \alpha_i (\dot{x}_0(t) - v_0(t) - \dots - v_i(t))^m$  for  $i \in \{1, 2, \dots, N\}$ .

Since equations of the form (3) are hard to analyse, we obtain sufficient conditions for their stability by analysing them in the neighbourhood of their equilibria. To that end, we note that  $v_i^* = 0$ ,  $i = 1, 2, \dots, N$  is an equilibrium for system (3). Linearising (3) about this equilibrium, we obtain

$$\dot{v}_i(t) = \beta_{i-1}^* v_{i-1}(t - \tau_{i-1}) - \beta_i^* v_i(t - \tau_i), \quad (4)$$

for  $i \in \{1, 2, \dots, N\}$ . Here,  $\beta_i^* = \alpha_i (\dot{x}_0)^m$  denotes the equilibrium coefficient for the  $i^{\text{th}}$  vehicle.

### III. THE NO-DELAY REGIME

In this section, we consider the idealistic case of drivers that can react instantaneously to stimuli. This results in zero reactions delays, and hence the linear model described by system (4) boils down to the following system of Ordinary Differential Equations (ODEs):

$$\dot{v}_i(t) = \beta_{i-1}^* v_{i-1}(t) - \beta_i^* v_i(t), \quad (5)$$

for  $i \in \{1, 2, \dots, N\}$ . This can be succinctly written in matrix form as follows:

$$\dot{\mathbf{V}}(t) = \mathbf{A}\mathbf{V}(t), \quad (6)$$

where  $\mathbf{V}(t) = [v_1(t) v_2(t) \dots v_N(t)]^T \in \mathbb{R}^N$ , and  $\mathbf{A} \in \mathbb{R}^{N \times N}$ . The matrix  $\mathbf{A}$ , known as the *dynamics matrix* [17, Section 2.2], is a lower-triangular matrix, given by:

$$A_{ij} = \begin{cases} -\beta_i^*, & i = j, \\ \beta_j^*, & i = j + 1, \\ 0, & \text{elsewhere.} \end{cases}$$

To characterise the stability of system (5), we require the eigenvalues of the dynamics matrix corresponding to system (6) to be negative [12, Theorem 5.1.1]. Since  $\mathbf{A}$  is a lower-triangular matrix, the characteristic polynomial is given by the product of the diagonal elements of the matrix  $(\lambda I - \mathbf{A})$  [13, Lemma 6.9.1]. Therefore, we have

$$f(\lambda) = \det(\lambda I - \mathbf{A}) = \prod_{i=1}^N (\lambda + \beta_i^*) = 0. \quad (7)$$

Therefore, the poles corresponding to system (5) are located at  $-\beta_i^*$ ,  $i \in \{1, 2, \dots, N\}$ . We note that, from physical constraints,  $\alpha_i > 0 \forall i$ . Also, since  $(\dot{x}_0)^m > 0$ ,  $\beta_i^* = \alpha_i (\dot{x}_0)^m > 0 \forall i$  for all physically relevant systems. Hence, the corresponding poles will lie in the open left-half of the Argand plane, thereby ensuring the stability of system (4) for all physically relevant values of the parameters.

### IV. THE SMALL-DELAY REGIME

In this section, we analyse system (3) in the small-delay regime. A way to obtain insights for small delays is to conduct a linearisation on time. Thus, we obtain a system of ODEs, which serves as an approximation to the original infinite-dimensional system (4), for small delays. We derive the criterion for this system of ODEs to be stable, thereby emphasising the design trade-off inherent among various system parameters and the reaction delay.

We begin by applying the Taylor series approximation to the time-delayed state variables thus:  $v_i(t - \tau_i) \approx v_i(t) - \tau_i \dot{v}_i(t)$ . Using this approximation for terms in (4), and re-arranging the resulting equations, we obtain

$$\dot{v}_i(t) + \frac{\beta_{i-1}^* \tau_{i-1}}{1 - \beta_i^* \tau_i} \dot{v}_{i-1}(t) = \frac{\beta_{i-1}^*}{1 - \beta_i^* \tau_i} v_{i-1}(t) - \frac{\beta_i^*}{1 - \beta_i^* \tau_i} v_{i-1}(t), \quad (8)$$

for  $i \in \{1, 2, \dots, N\}$ . This can be succinctly written in matrix form as

$$B\dot{\mathbf{V}}(t) = \mathbf{A}\mathbf{V}(t), \quad (9)$$

where  $\mathbf{V}(t) = [v_1(t) v_2(t) \cdots v_N(t)]^T \in \mathbb{R}^N$ . The matrix  $A$  is as defined in Section III, and  $B$  is given by

$$B_{ij} = \begin{cases} 1, & i = j, \\ \frac{-\beta_i^* \tau_i}{1 - \beta_j^* \tau_j}, & i = j + 1, \\ 0, & \text{elsewhere.} \end{cases}$$

We note that  $B$  is a lower-triangular matrix with unit diagonal entries. Hence, it is invertible, and the inverse is also a lower-triangular matrix having unit diagonal elements. Further, since  $A$  is a lower-triangular matrix as well, the dynamics matrix corresponding to system (8), *i.e.*,  $\tilde{A} = B^{-1}A$ , is a lower-triangular matrix since it is the product of two lower-triangular matrices [11, Section 1.4]. Further, due to the said structures, the diagonal elements of  $\tilde{A}$  are given by

$$\tilde{A}_{11} = \frac{\beta_1^*}{1 - \beta_1^* \tau_1}, \text{ and } \tilde{A}_{ii} = \frac{\beta_{i-1}^*}{1 - \beta_i^* \tau_1}, \quad i > 1. \quad (10)$$

Therefore, the characteristic polynomial corresponding to system (8) is the product of the diagonal entries of the matrix  $(\lambda I - \tilde{A})$  [13, Lemma 6.9.1]. That is,

$$f(\lambda) = \det(\lambda I - \tilde{A}) = \prod_{i=1}^N (\lambda + \tilde{A}_{ii}) = 0. \quad (11)$$

This shows that the poles of system (8) are located at  $-\tilde{A}_{ii}$ ,  $i \in \{1, 2, \dots, N\}$ . Hence, for system (8) to be stable, the diagonal entries of its dynamics matrix  $\tilde{A}$  have to be positive. From (10), this is satisfied if and only if

$$\beta_i^* \tau_i < 1, \quad i \in \{1, 2, \dots, N\}. \quad (12)$$

Hence, the above equation represents the necessary and sufficient condition for stability of the time-linearised system (8). Further, as noted in Section II, (12) is a sufficient condition for the local stability of the RCCFM, described by system (3).

## V. THE HOPF BIFURCATION

Having studied system (3) in the no-delay and the small-delay regimes, in this section, we focus on the arbitrary-delay regime. We derive the necessary and sufficient condition for the local stability of system (3), and show that the corresponding traffic flow transits from the locally stable to the unstable regime via a Hopf bifurcation [2].

### A. Transversality condition

Hopf bifurcation is a phenomenon wherein a system undergoes a stability switch due to a pair of conjugate eigenvalues crossing the imaginary axis in the Argand plane [14, Chapter 11, Theorem 1.1]. Mathematically, a Hopf bifurcation analysis is a rigorous way of proving the emergence of limit cycles in non-linear dynamical systems.

In order to ascertain whether system (3) undergoes a stability loss via a Hopf bifurcation, we follow [10] and introduce an exogenous, non-dimensional parameter  $\kappa$ . A general system of delay differential equations  $\dot{x}(t) =$

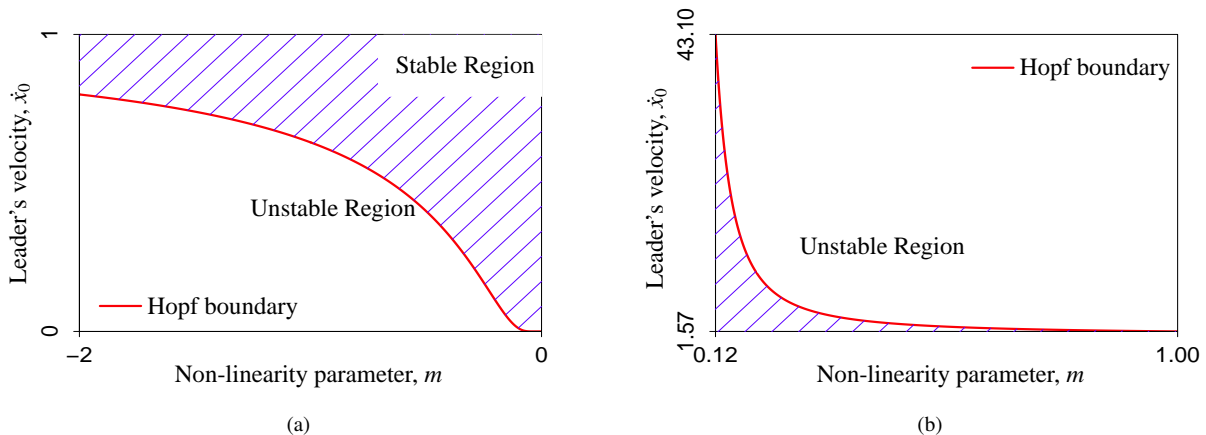


Fig. 1: The stability regions for the RCCFM are depicted, separated by the Hopf boundary; a visual representation of (20) with  $c = 1$ , where  $\kappa$  is set to unity. The shaded areas represent the stable regions. (a) is for  $m < 0$ , whereas (b) is for  $m > 0$ . Pictorially, we restrict  $m \in [0.12, 1]$  for clarity of visual representation. For  $m = 0$ , the system is stable for all values of the leader's equilibrium velocity since  $c < \pi/2$ .

$f(x(t), x(t - \tau_1), \dots, x(t - \tau_n))$  is modified to  $\dot{x}(t) = \kappa f(x(t), x(t - \tau_1), \dots, x(t - \tau_n))$  with the introduction of the exogenous parameter. In the specific case of the RCCFM, introducing  $\kappa$  in (3) results in

$$\dot{v}_i(t) = \kappa \beta_{i-1}(t - \tau_{i-1}) v_{i-1}(t - \tau_{i-1}) - \kappa \beta_i(t - \tau_i) v_i(t - \tau_i), \quad (13)$$

for each  $i \in \{1, 2, \dots, N\}$ . We linearise this about the all-zero equilibrium to obtain

$$\dot{v}_i(t) = \kappa \beta_{i-1}^* v_{i-1}(t - \tau_{i-1}) - \kappa \beta_i^* v_i(t - \tau_i), \quad (14)$$

for  $i \in \{1, 2, \dots, N\}$ . The characteristic equation pertaining to (14) is [8, Equation (15)]

$$\lambda + \kappa \beta_i^* e^{-\lambda \tau_i} = 0. \quad (15)$$

It is well known that for (14) to be stable, all the roots of (15) must lie in the open-left half of the Argand plane [12, Theorem 5.1.1]. Hence, to analyse the local stability of system (13), we search for a conjugate pair of eigenvalues of (15) that crosses the imaginary axis in the Argand plane, thereby pushing the system into an unstable regime. To that end, we substitute  $\lambda = j\omega$ , with  $j = \sqrt{-1}$ , in (15) to obtain

$$\kappa \beta_i^* \cos(\omega \tau_i) = 0, \text{ and } \omega - \kappa \beta_i^* \sin(\omega \tau_i) = 0.$$

The first equality implies  $\omega \tau_i = (2n + 1)\frac{\pi}{2}$  for  $n = 0, 1, 2, \dots$ . Using this, the second equality then results in  $\kappa \beta_i^* = \omega$  for  $n = 0, 2, 4, \dots$ . Therefore, when a conjugate pair of eigenvalues is on the imaginary axis in the Argand

plane, we have

$$\omega_0 = (2n + 1) \frac{\pi}{2\tau_i}, \quad n = 0, 1, 2, \dots, \quad (16)$$

$$\kappa_{cr} = (2n + 1) \frac{\pi}{2\beta_i^* \tau_i}, \quad n = 0, 2, 4, \dots, \quad (17)$$

where  $\kappa_{cr}$  is the critical value of  $\kappa$  at  $\omega = \omega_0$ .

To show that system (13) undergoes a Hopf bifurcation at  $\kappa = \kappa_{cr}$  for each  $n \in \{0, 2, 4, \dots\}$ , we need to prove the transversality condition of the Hopf spectrum. That is, we must show that [14, Chapter 11, Theorem 1.1]

$$\text{Real} \left( \frac{d\lambda}{d\kappa} \right)_{\kappa=\kappa_{cr}} \neq 0 \quad (18)$$

holds for each  $n \in \{0, 2, 4, \dots\}$ . Therefore, we differentiate (15) with respect to  $\kappa$ . Algebraic manipulations then yield

$$\text{Real} \left( \frac{d\lambda}{d\kappa} \right)_{\kappa=\kappa_{cr}} = \frac{2\beta_i^* \tau_i^2 \omega_0^2}{(2n + 1)(1 + \tau_i^2 \omega_0^2)\pi} > 0, \quad (19)$$

for  $n \in \{0, 2, 4, \dots\}$ . This implies that system (13) undergoes a Hopf bifurcation at  $\kappa = \kappa_{cr}$  for each  $n \in \{0, 2, 4, \dots\}$ . Hence,  $\kappa < \kappa_{cr}$  is the necessary and sufficient condition for system (13) to be locally stable.

First, we remark that  $\kappa = \kappa_{cr}$  is the equation of the stability boundary, also known as the Hopf boundary. Once we obtain the expression for  $\kappa_{cr}$ , we tune the system parameters such that the non-dimensional parameter is unity on the stability boundary, *i.e.*, we set  $2\beta_i^* \tau_i = \pi$  to make  $\kappa_{cr}$  unity. Next, we note that the system loses stability when the very first conjugate pair of eigenvalues, corresponding to  $n = 0$  in (17), crosses the imaginary axis. Further increase in  $\kappa$  cannot restore system stability – indeed, the derivative in (19) is positive for each  $n \in \{0, 2, 4, \dots\}$ . That is, an increase in  $\kappa$  results in the eigenvalues moving to the right in the Argand plane, making it impossible to regain stability. Lastly, it is clear from (17) that  $\alpha_i$  and  $\tau_i$  are inversely related on the Hopf boundary, *i.e.*, when  $\kappa_{cr} = 1$ . Hence, we set  $\alpha_i \tau_i = c$ , a Real constant, in order to study the trade-off between the leader's profile  $\dot{x}_0$ , and the non-linearity parameter  $m$ . The resulting necessary and sufficient condition for the local stability of system (3) is

$$(\dot{x}_0)^m < \frac{\pi}{2c}. \quad (20)$$

When  $m = 0$ , the system would be stable if  $c < \pi/2$ . When  $m > 0$ , (20) applies verbatim. When  $m < 0$ ,  $(\dot{x}_0)^{|m|} > 2c/\pi$  characterises the system stability. The system exhibits qualitatively different behaviour for  $c < \pi/2$  and  $c > \pi/2$ . The stability chart, a plot depicting the Hopf boundary as the non-linearity parameter  $m$  varies, is as shown in Figs 1a and 1b for  $c < \pi/2$ . It can be observed that there is a qualitative change in the system behaviour as  $m$  changes sign. For  $m < 0$ , fast lead vehicles stabilise the system, while for  $m > 0$ , slow lead vehicles are required to ensure system stability. From (20), we observe that when  $c > \pi/2$ , slow lead vehicles stabilise the system when  $m < 0$ , and fast lead vehicles stabilise the system when  $m > 0$ .

## B. Discussion

A few comments are in order.

- (1) As pointed out in the introduction, the limit cycles that emerge due to a Hopf bifurcation physically manifest themselves as of back-propagating congestion wave, known as a ‘phantom jam.’ Therefore, the foregoing analysis offers a possible explanation of a commonly-observed phenomenon.
- (2) We note that the non-dimensional parameter  $\kappa$  introduced in Section V-A is not a model parameter; it is an exogenous mathematical entity to aid the analysis. Its usefulness is at the edge of the stability boundary, wherein it is used to push the system into the unstable regime in a controlled manner, as described in the analysis.
- (3) It is well known in the control literature that a suitable variation in gain parameter can destabilise a system [23, Section 3.7]. Hence, to ensure that the bifurcation phenomenon is not an artefact of the exogenous parameter, it is required to verify that the transversality condition of the Hopf spectrum is satisfied for at least one model parameter beforehand. For the case of the RCCFM, following the derivation in Section V-A, it is easy to prove that the RCCFM could undergo a Hopf bifurcation due to an appropriate variation in any of  $\alpha_i$ ,  $\tau_i$ ,  $\dot{x}_0$  or  $m$ .
- (4) Substituting  $n = 0$  in (17), and letting  $\kappa = 1$  on the stability boundary, the necessary and sufficient condition for the local stability of system (3) becomes

$$\beta_i^* \tau_i < \frac{\pi}{2}. \quad (21)$$

We notice that this simple condition coincides with the sufficient condition derived in [8, Equation (12)]. Furthermore, we note that when  $\tau_i = 0$ , (21) is trivially satisfied. This, in turn, validates the result derived in Section III. Also, notice that the region in the parameter space described by (12) is a strict subset of the region described by (21). This validates the fact that (12) is a sufficient condition for the local stability of system (3).

- (5) In this work, we consider the  $l = 0$  case for the following reason. While the CCFM described by (2) for  $l \neq 0$  satisfies the transversality condition, it need not undergo only a Hopf bifurcation. Indeed, the case  $l \neq 0$  appears to be more involved and merits further investigation.

## VI. NON-OSCILLATORY CONVERGENCE

In previous sections, we focused on deriving a necessary as well as the necessary and sufficient conditions for the local stability of system (3). In the next two sections, we explore two important properties of the stable region; namely, non-oscillatory convergence and the rate of convergence.

In this section, we characterise the region of non-oscillatory convergence. Mathematically, this amounts to ensuring that the poles corresponding to system (3) are negative real numbers. Qualitatively, non-oscillatory convergence avoids jerky vehicular motion since relative velocities and headways constitute dynamical variables. Such results could help ensure the smooth flow of traffic, and hence improve the ride quality.

In the above spirit, following [26], we derive the necessary and sufficient condition for non-oscillatory convergence of system (3). The characteristic equation pertaining to system (4), after dropping the subscript ‘ $i$ ’ for convenience,

is  $f(\lambda) = \lambda + \beta^* e^{-\lambda\tau} = 0$  [8, Equation (8)]. Substituting  $\lambda = -\sigma - j\omega$  and simplifying, we obtain

$$\begin{aligned}\sigma &= \beta^* e^{\sigma\tau} \cos(\omega\tau), \\ \omega &= \beta^* e^{\sigma\tau} \sin(\omega\tau).\end{aligned}\tag{22}$$

These, in turn, yield  $\tan(\omega\tau) = \omega/\sigma$ . To ensure that  $\omega = 0$  is the only solution of this equation, the necessary and sufficient condition is  $\sigma\tau \geq 1$ . Re-writing (22), we have

$$\beta^* \tau e^{\sigma\tau} \left( \frac{\sin(\omega\tau)}{\omega\tau} \right) = 1.$$

In the limit  $\omega \rightarrow 0$ , the term within the brackets represents  $\text{sinc}(0) = 1$ . Moreover, the exponential term is bounded by  $e$  since  $\sigma\tau \geq 1$ . Hence, the boundary of non-oscillatory convergence is  $\beta^* \tau e = 1$ , and the corresponding necessary and sufficient condition for non-oscillatory convergence is

$$\beta^* \tau \leq \frac{1}{e}.\tag{23}$$

Notice that the region in the parameter space described by (23) is a strict subset of the region described by (21). Therefore, from these two equations, we can summarise the conditions for the local stability of system (3) as follows.

- (1) If  $\beta^* \tau \in [0, \pi/2)$ , the system is locally stable.
- (2) Additionally, if  $\beta^* \tau \in [0, 1/e]$ , the system converges to the equilibrium in a non-oscillatory fashion.
- (3) Contrarily, if  $\beta^* \tau \in (1/e, \pi/2)$ , the system is locally stable. However, the state variable oscillates about the equilibrium, converging to it asymptotically.

## VII. RATE OF CONVERGENCE

Rate of convergence is an important performance metric that dictates the time a dynamical system takes to equilibrate, when perturbed. In the context of a transportation network, it is related to the time required to attain

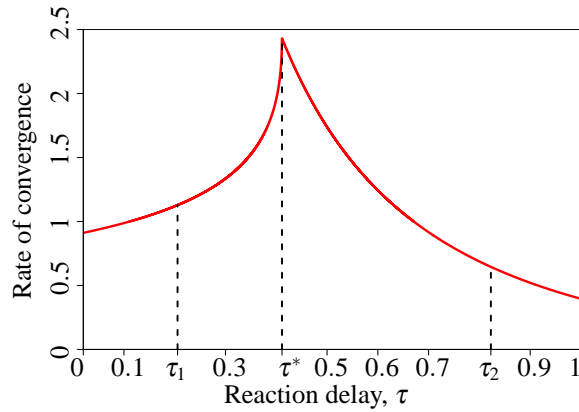


Fig. 2: Figure portraying the variation of the rate of convergence of the RCCFM as the reaction delay is varied.

the uniform traffic flow, once the traffic flow is perturbed (by events such as the departure of a vehicle from the platoon). Following [7], we characterise the rate of convergence for the RCCFM.

The characteristic equation pertaining to system (4), with the subscript ‘ $i$ ’ dropped for ease of exposition, is  $f(\lambda) = \lambda + \beta^* e^{-\lambda\tau} = 0$  [8, Equation (8)]. In time domain, this corresponds to a system  $\dot{x}(t) = -\beta^* x(t - \tau)$ , where  $x$  is an arbitrarily chosen dynamical variable. The rate of convergence of such a system is the reciprocal of the smallest among  $\sigma_1$ ,  $\sigma_2$  and  $\sigma_3$ , where these quantities are obtained by solving the equations [7, Theorem 2]

$$\begin{aligned}\sigma\tau &= 1, \\ \sigma\tau e^{-\sigma\tau} &= -\beta^*\tau, \\ \frac{m}{\sin(m)} e^{-\frac{m}{\tan(m)}} &= -\beta^*\tau, \quad m = \sigma\tau \tan(m),\end{aligned}$$

respectively. The rate of convergence is maximum at  $\tau^* = 1/(\beta^*e)$ . For  $\tau < \tau^*$ , the rate of convergence increases, whereas it decreases for  $\tau > \tau^*$  [7].

We solve the above equations using MATLAB to illustrate the variations in the rate of convergence for the RCCFM, as the reaction delay is varied. To that end, we consider a tagged vehicle following a lead vehicle with an equilibrium velocity of 5 m/s. The tagged vehicle has a sensitivity coefficient of  $\alpha = 0.4 \text{ s}^{-1}$ , and we let  $m = 0.5$ . Therefore,  $\tau^* = 0.4113 \text{ s}$ .

The rate of convergence for this system is plotted in Fig. 2. It can be seen that the rate of convergence increases with  $\tau$  for  $\tau < \tau^*$ , and decreases when the reaction delay is varied beyond  $\tau^*$ . Also, note that the condition for the maximum rate of convergence coincides with the boundary for non-oscillatory convergence of the RCCFM,  $\beta^*\tau e = 1$ . Hence, it would be optimal to choose parameters satisfying this equation.

However, in practise, system parameters may vary. This will result in a shift of the operating point of the RCCFM, and may result in a trade-off between the rate of convergence and non-oscillatory convergence of the RCCFM. Notice that Fig. 3 depicts this trade-off, which is due to the lack of symmetry about  $\tau^*$ . In the vicinity of  $\tau^*$ , if the operating point of the RCCFM shifts to the left of  $\tau^*$ , then the system retains its non-oscillatory behaviour and the rate of convergence reduces drastically. On the other hand, if the operating point of the RCCFM shifts to the right of  $\tau^*$  in its vicinity, then the system converges to the equilibrium in an oscillatory fashion, but at a relatively faster rate. However, if the reaction delay increases considerably beyond  $\tau^*$ , then not only does the system exhibit oscillatory convergence, it may also converge to the equilibrium very slowly. This is portrayed in Fig. 2 using  $\tau_1 = \tau^*/2$  and  $\tau_2 = 2\tau^*$ . Clearly, the rate of convergence at  $\tau_2$  is considerably lesser than that at  $\tau_1$ .

We note that the characteristic equation captures the closed-loop pairwise interaction in the platoon. Hence, if we denote by  $t_i^e$  the time take by the  $i^{th}$  pair to equilibrate, then the time taken by the platoon to equilibrate following a perturbation, denoted by  $T_{RCCFM}^e$ , will be given by

$$T_{RCCFM}^e = \sum_{i=1}^N t_i^e. \quad (24)$$

It is clear that (24) is an upper bound on the time taken by the platoon to equilibrate. However, the equality holds since the  $i^{th}$  pair cannot equilibrate till the  $(i-1)^{th}$  pair has reached its equilibrium.

### VIII. HOPF BIFURCATION ANALYSIS

In the previous sections, we have characterised the stable region for the RCCFM, and studied two of its most important properties; namely, region of non-oscillatory convergence and the rate of convergence. We have also proved, by means of the transversality condition of the Hopf spectrum (19), that system (3) loses stability via a Hopf bifurcation. In this section, we study the RCCFM when it is pushed just beyond the stable region. We characterise the *type* of the bifurcation and the *asymptotic orbital stability* of the emergent limit cycles, following closely the style of analysis presented in [2], by using Poincaré normal forms and the center manifold theory.

We begin by denoting the RHS of (13) as  $f_i$ . That is, for  $i \in \{1, 2, \dots, N\}$ ,

$$f_i \triangleq \kappa\beta_{i-1}(t - \tau_{i-1})v_{i-1}(t - \tau_{i-1}) - \kappa\beta_i(t - \tau_i)v_i(t - \tau_i). \quad (25)$$

Let  $\mu = \kappa - \kappa_{cr}$ . Observe that the system undergoes a Hopf bifurcation at  $\mu = 0$ , where  $\kappa = \kappa_{cr}$ . Henceforth, we consider  $\mu$  as the bifurcation parameter. An incremental change in  $\kappa$  from  $\kappa_{cr}$  to  $\kappa_{cr} + \mu$ , where  $\mu > 0$ , pushes the system in to its unstable regime. We now provide a concise step-by-step overview of the detailed local bifurcation analysis, before delving into the technical details.

*Step 1:* Using Taylor series expansion, we segregate the RHS of (25) into linear and non-linear parts. We then cast this into the standard form of an Operator Differential Equation (OpDE).

*Step 2:* At the critical value of the bifurcation parameter, *i.e.*, at  $\mu = 0$ , the system has exactly one pair of purely imaginary eigenvalues with non-zero angular velocity, as given by (16). The linear eigenspace spanned by the corresponding eigenvectors is called the critical eigenspace. The center manifold theorem [2] guarantees the existence of a locally invariant 2-dimensional manifold that is a tangent to the critical eigenspace at the equilibrium of the system.

*Step 3:* Next, we project the system onto its critical eigenspace as well as its complement, at the critical value of the bifurcation parameter. This helps describe the dynamics of the system on the center manifold, with the aid of an ODE in a single complex variable.

*Step 4:* Finally, using Poincaré normal forms, we evaluate the Lyapunov coefficient and the Floquet exponent, which characterise the type of the Hopf bifurcation and the asymptotic orbital stability of the emergent limit cycles respectively.

We begin the analysis by expanding (25) about the all-zero equilibrium using Taylor's series, to obtain

$$\begin{aligned} \dot{v}_i(t) = & -\kappa\beta_i^*v_{i,t}(-\tau_i) + \kappa\beta_{i-1}^*v_{(i-1),t}(-\tau_{i-1}) + \left(\frac{2\kappa m\beta_i^*}{\dot{x}_0}\right) \sum_{l=1}^i v_{l,t}(-\tau_i)v_{i,t}(-\tau_i) \\ & - \left(\frac{2\kappa m\beta_{i-1}^*}{\dot{x}_0}\right) \sum_{l=1}^{i-1} v_{l,t}(-\tau_{i-1})v_{(i-1),t}(-\tau_{i-1}) - \left(\frac{12\kappa m(m-1)\beta_i^*}{\dot{x}_0^2}\right) \sum_{n=1}^i \sum_{l=1}^i v_{l,t}(-\tau_i)v_{n,t}(-\tau_i)v_{i,t}(-\tau_i) \\ & + \left(\frac{12\kappa m(m-1)\beta_{i-1}^*}{\dot{x}_0^2}\right) \sum_{n=1}^{i-1} \sum_{l=1}^{i-1} v_{l,t}(-\tau_{i-1})v_{n,t}(-\tau_{i-1})v_{(i-1),t}(-\tau_{i-1}) + \text{higher order terms}, \quad (26) \end{aligned}$$

where we use the shorthand  $v_{i,t}(-\tau_i)$  to represent  $v_i(t - \tau_i)$ .

In the following, we use  $\mathcal{C}^k(A; B)$  to denote the linear space of all functions from  $A$  to  $B$  which are  $k$  times differentiable, with each derivative being continuous. Also, we use  $\mathcal{C}$  to denote  $\mathcal{C}^0$ , for convenience.

We define  $\mathbf{V}(t) \triangleq [v_1(t) \ v_2(t) \ \cdots \ v_N(t)]^T$ , and note that (13) is of the form:

$$\frac{d\mathbf{V}(t)}{dt} = \mathcal{L}_\mu \mathbf{V}_t(\theta) + \mathcal{F}(\mathbf{V}_t(\theta), \mu), \quad (27)$$

where  $t > 0$ ,  $\mu \in \mathbb{R}$ , and where for  $\tau = \max_i \tau_i > 0$ ,

$$\mathbf{V}_t(\theta) = \mathbf{V}(t + \theta), \quad \mathbf{V} : [-\tau, 0] \longrightarrow \mathbb{R}^N, \quad \theta \in [-\tau, 0].$$

Here,  $\mathcal{L}_\mu : \mathcal{C}([-\tau, 0]; \mathbb{R}^N) \longrightarrow \mathbb{R}^N$  is a one-parameter family of continuous, bounded linear functionals, whereas the operator  $\mathcal{F} : \mathcal{C}([-\tau, 0]; \mathbb{R}^N) \longrightarrow \mathbb{R}^N$  is an aggregation of the non-linear terms. Further, we assume that  $\mathcal{F}(\mathbf{V}_t, \mu)$  is analytic, and that  $\mathcal{F}$  and  $\mathcal{L}_\mu$  depend analytically on the bifurcation parameter  $\mu$ , for small  $|\mu|$ . The objective now is to cast (27) in the standard form of an OpDE:

$$\frac{d\mathbf{V}_t}{dt} = \mathcal{A}(\mu)\mathbf{V}_t + \mathcal{R}\mathbf{V}_t, \quad (28)$$

since the dependence here is on  $\mathbf{V}_t$  alone rather than both  $\mathbf{V}_t$  and  $\mathbf{V}(t)$ . To that end, we begin by transforming the linear problem  $d\mathbf{V}(t)/dt = \mathcal{L}_\mu \mathbf{V}_t(\theta)$ . We note that, by the *Riesz representation theorem* [29, Theorem 6.19], there exists an  $N \times N$  matrix-valued measure  $\eta(\cdot, \mu) : \mathcal{B}(\mathcal{C}([-\tau, 0]; \mathbb{R}^N)) \longrightarrow \mathbb{R}^{N \times N}$ , wherein each component of  $\eta(\cdot)$  has bounded variation, and for all  $\phi \in \mathcal{C}([-\tau, 0]; \mathbb{R}^N)$ , we have

$$\mathcal{L}_\mu \phi = \int_{-\tau}^0 d\eta(\theta, \mu) \phi(\theta). \quad (29)$$

In particular,

$$\mathcal{L}_\mu \mathbf{V}_t = \int_{-\tau}^0 d\eta(\theta, \mu) \mathbf{V}(t + \theta).$$

Motivated by the linearised system (14), we define

$$(\mathbf{d}\eta)_{ij} = \begin{cases} -\kappa\beta_i^* \delta(\theta + \tau_i), & i = j, \\ \kappa\beta_j^* \delta(\theta + \tau_j), & j = i - 1, i > 1, \\ 0. & \text{otherwise,} \end{cases}$$

where  $\delta(\cdot)$  denotes the Dirac delta. Observe that  $\mathbf{d}\eta = (\mathbf{d}\eta)_{i,j=1}^N \mathbf{d}\theta$  as defined above satisfies (29). For instance, when  $N = 4$ , we have

$$\mathbf{d}\eta = \begin{bmatrix} -\kappa\beta_1^* \delta(\theta + \tau_1) & 0 & 0 & 0 \\ \kappa\beta_1^* \delta(\theta + \tau_1) & -\kappa\beta_2^* \delta(\theta + \tau_2) & 0 & 0 \\ 0 & \kappa\beta_2^* \delta(\theta + \tau_2) & -\kappa\beta_3^* \delta(\theta + \tau_3) & 0 \\ 0 & 0 & \kappa\beta_3^* \delta(\theta + \tau_3) & -\kappa\beta_4^* \delta(\theta + \tau_4) \end{bmatrix} \mathbf{d}\theta.$$

For  $\phi \in \mathcal{C}^1([-\tau, 0]; \mathbb{C}^N)$ , we define

$$\mathcal{A}(\mu)\phi(\theta) = \begin{cases} \frac{d\phi(\theta)}{d\theta}, & \theta \in [-\tau, 0), \\ 0 \\ \int_{-\tau}^{\theta} d\eta(s, \mu)\phi(s) \equiv \mathcal{L}\mu, & \theta = 0, \end{cases} \quad (30)$$

and

$$\mathcal{R}\phi(\theta) = \begin{cases} 0, & \theta \in [-\tau, 0), \\ \mathcal{F}(\phi, \mu), & \theta = 0. \end{cases}$$

With the above definitions, we observe that  $d\mathbf{V}_t/d\theta \equiv d\mathbf{V}_t/dt$ . Hence, we have successfully cast (27) in the form of (28). To obtain the required coefficients, it is sufficient to evaluate various expressions for  $\mu = 0$ , which we use henceforth. We start by finding the eigenvector of the operator  $\mathcal{A}(0)$  with eigenvalue  $\lambda(0) = j\omega_0$ . That is, we want an  $N \times 1$  vector (to be denoted by  $q(\theta)$ ) with the property that  $\mathcal{A}(0)q(\theta) = j\omega_0 q(\theta)$ . We assume the form:  $q(\theta) = [1 \ \phi_1 \ \phi_2 \ \cdots \ \phi_{N-1}]^T e^{j\omega_0\theta}$ , and solve the eigenvalue equation to obtain

$$\begin{bmatrix} -\kappa\beta_1^* e^{-j\omega_0\tau_1} \\ \kappa\beta_1^* e^{-j\omega_0\tau_1} - \kappa\beta_2^* e^{-j\omega_0\tau_2} \phi_1 \\ \kappa\beta_2^* e^{-j\omega_0\tau_2} \phi_1 - \kappa\beta_3^* e^{-j\omega_0\tau_3} \phi_2 \\ \vdots \\ \kappa\beta_{N-2}^* e^{-j\omega_0\tau_{N-2}} \phi_{N-3} - \kappa\beta_{N-1}^* e^{-j\omega_0\tau_{N-1}} \phi_{N-2} \\ \kappa\beta_{N-1}^* e^{-j\omega_0\tau_{N-1}} \phi_{N-2} - \kappa\beta_N^* e^{-j\omega_0\tau_N} \phi_{N-1} \end{bmatrix} = j\omega_0 \begin{bmatrix} 1 \\ \phi_1 \\ \phi_2 \\ \vdots \\ \phi_{N-2} \\ \phi_{N-1} \end{bmatrix}.$$

On simplification, for  $i \in \{1, 2, \dots, N-1\}$ , we obtain

$$\phi_i = \frac{\kappa\beta_i^* e^{-j\omega_0\tau_i}}{j\omega_0 + \kappa\beta_{i+1}^* e^{-j\omega_0\tau_{i+1}}} \phi_{i-1},$$

where we set  $\phi_0 = 1$  for notational brevity.

We define the *adjoint* operator as follows:

$$\mathcal{A}^*(0)\phi(\theta) = \begin{cases} -\frac{d\phi(\theta)}{d\theta}, & \theta \in (0, \tau], \\ 0 \\ \int_{-\tau}^{\theta} d\eta^T(s, 0)\phi(-s), & \theta = 0, \end{cases}$$

where  $d\eta^T$  is the transpose of  $d\eta$ . We note that the domains of  $\mathcal{A}$  and  $\mathcal{A}^*$  are  $\mathcal{C}^1([-\tau, 0]; \mathbb{C}^N)$  and  $\mathcal{C}^1([0, \tau]; \mathbb{C}^N)$  respectively. Therefore, if  $j\omega_0$  is an eigenvalue of  $\mathcal{A}$ , then  $-j\omega_0$  is an eigenvalue of  $\mathcal{A}^*$ . Hence, to find the eigenvector of  $\mathcal{A}^*(0)$  corresponding to  $-j\omega_0$  (to be denoted by  $p(\theta)$ ), we assume the form:  $p(\theta) = B[\psi_{N-1} \ \psi_{N-2} \ \psi_{N-3} \ \cdots \ 1]^T e^{j\omega_0\theta}$ , and solve  $\mathcal{A}^*(0)p(\theta) = -j\omega_0 p(\theta)$  to obtain

$$\begin{bmatrix} -\kappa\beta_1^* e^{j\omega_0\tau_1} \psi_{N-1} + \kappa\beta_1^* e^{j\omega_0\tau_1} \psi_{N-2} \\ -\kappa\beta_2^* e^{j\omega_0\tau_2} \psi_{N-2} + \kappa\beta_2^* e^{j\omega_0\tau_2} \psi_{N-3} \\ \vdots \\ -\kappa\beta_{N-1}^* e^{j\omega_0\tau_{N-1}} \psi_1 + \kappa\beta_{N-1}^* e^{j\omega_0\tau_{N-1}} \\ -\kappa\beta_N^* e^{j\omega_0\tau_N} \end{bmatrix} = -j\omega_0 \begin{bmatrix} \psi_{N-1} \\ \psi_{N-2} \\ \vdots \\ \psi_1 \\ 1 \end{bmatrix}.$$

On simplification, for  $i \in \{1, 2, \dots, N-1\}$ , we obtain

$$\psi_i = \frac{\kappa_i \beta_{N-i}^* e^{j\omega_0 \tau_{N-i}}}{\kappa_i \beta_{N-i}^* e^{j\omega_0 \tau_{N-i}} - j\omega_0} \psi_{i-1},$$

where we set  $\psi_0 = 1$  for notational brevity.

Further, the normalisation condition for Hopf bifurcation requires that  $\langle p, q \rangle = 1$ , thus yielding an expression for  $B$ .

For any  $q \in \mathcal{C}([- \tau, 0]; \mathbb{C}^N)$  and  $p \in \mathcal{C}([0, \tau]; \mathbb{C}^N)$ , the inner product is defined as

$$\langle p, q \rangle \triangleq \bar{p} \cdot q - \int_{\theta=-\tau}^0 \int_{\zeta=0}^{\theta} \bar{p}^T(\zeta - \theta) d\eta q(\zeta) d\zeta, \quad (31)$$

where the overbar represents the complex conjugate and the “ $\cdot$ ” represents the regular dot product. The first term in the RHS of (31) can be simplified to

$$\bar{p} \cdot q = \bar{B} \left( \sum_{k=0}^{N-1} \bar{\psi}_{N-1-k} \phi_k \right),$$

where, as before,  $\phi_0 = \psi_0 = 1$ . The integrand in the second term of the RHS in (31) reduces to

$$\bar{B} \kappa e^{j\omega_0 \theta} \left[ \sum_{n=1}^N (\beta_n^* \delta(\theta + \tau_n) \phi_{n-1} (\bar{\psi}_{N-n-1} - \bar{\psi}_{N-n})) \right] d\theta,$$

with the dummy variable  $\psi_{-1} = 0$  used for notational brevity. On integrating this term, we obtain

$$\bar{B} \kappa \left[ \sum_{n=1}^N (\beta_n^* \tau_n e^{-j\omega_0 \tau_n} \phi_{n-1} (\bar{\psi}_{N-n} - \bar{\psi}_{N-n-1})) \right].$$

Substituting the two terms in (31), equating the resulting term to unity, and simplifying, we obtain

$$\bar{B} = \frac{1}{\zeta_1 + \zeta_2}, \quad \text{where, } \zeta_1 = \sum_{k=0}^{N-1} \bar{\psi}_{N-1-k} \phi_k, \quad \text{and } \zeta_2 = \sum_{n=1}^N (\kappa_i \beta_n^* \tau_n e^{-j\omega_0 \tau_n} \phi_{n-1} (\bar{\psi}_{N-n} - \bar{\psi}_{N-n-1})).$$

For  $\mathbf{V}_t$ , a solution of (28) at  $\mu = 0$ , we define

$$z(t) = \langle p(\theta), \mathbf{V}_t \rangle, \quad \text{and,}$$

$$\mathbf{w}(t, \theta) = \mathbf{V}_t(\theta) - 2\text{Real}(z(t)q(\theta)).$$

Then, on the center manifold  $C_0$ , we have  $\mathbf{w}(t, \theta) = \mathbf{w}(z(t), \bar{z}(t), \theta)$ , where

$$\mathbf{w}(z(t), \bar{z}(t), \theta) = \mathbf{w}_{20}(\theta) \frac{z^2}{2} + \mathbf{w}_{02}(\theta) \frac{\bar{z}^2}{2} + \mathbf{w}_{11}(\theta) z \bar{z} + \dots \quad (32)$$

Effectively,  $z$  and  $\bar{z}$  are the local coordinates for  $C_0$  in  $\mathcal{C}$  in the directions of  $p$  and  $\bar{p}$  respectively. We note that  $\mathbf{w}$  is real if  $\mathbf{V}_t$  is real, and we deal only with real solutions. The existence of the center manifold  $C_0$  enables the reduction of (28) to an ODE in a single complex variable on  $C_0$ . At  $\mu = 0$ , the said ODE can be described as

$$\begin{aligned} \dot{z}(t) &= \langle p, \mathcal{A}\mathbf{V}_t + \mathcal{R}\mathbf{V}_t \rangle, \\ &= j\omega_0 z(t) + \bar{p}(0) \cdot \mathcal{F}(\mathbf{w}(z, \bar{z}, \theta) + 2\text{Real}(z(t)q(\theta))), \\ &= j\omega_0 z(t) + \bar{p}(0) \cdot \mathcal{F}_0(z, \bar{z}). \end{aligned} \quad (33)$$

This is written in abbreviated form as

$$\dot{z}(t) = j\omega_0 z(t) + g(z, \bar{z}). \quad (34)$$

The objective now is to expand  $g$  in powers of  $z$  and  $\bar{z}$ . However, this requires  $\mathbf{w}_{ij}(\theta)$ 's from (32). Once these are evaluated, the ODE (33) for  $z$  would be explicit (as given by (34)), where  $g$  can be expanded in terms of  $z$  and  $\bar{z}$  as

$$g(z, \bar{z}) = \bar{p}(0) \cdot \mathcal{F}_0(z, \bar{z}) = g_{20} \frac{z^2}{2} + g_{02} \frac{\bar{z}^2}{2} + g_{11} z\bar{z} + g_{21} \frac{z^2 \bar{z}}{2} + \dots \quad (35)$$

Next, we write  $\dot{\mathbf{w}} = \dot{\mathbf{V}}_t - \dot{z}q - \dot{\bar{z}}\bar{q}$ . Using (28) and (34), we then obtain the following ODE:

$$\dot{\mathbf{w}} = \begin{cases} \mathcal{A}\mathbf{w} - 2\text{Real}(\bar{p}(0) \cdot \mathcal{F}_0 q(\theta)), & \theta \in [-\tau, 0), \\ \mathcal{A}\mathbf{w} - 2\text{Real}(\bar{p}(0) \cdot \mathcal{F}_0 q(0)) + \mathcal{F}_0, & \theta = 0. \end{cases}$$

This can be re-written using (32) as

$$\dot{\mathbf{w}} = \mathcal{A}\mathbf{w} + H(z, \bar{z}, \theta), \quad (36)$$

where  $H$  can be expanded as

$$H(z, \bar{z}, \theta) = H_{20}(\theta) \frac{z^2}{2} + H_{02}(\theta) \frac{\bar{z}^2}{2} + H_{11}(\theta) z\bar{z} + H_{21}(\theta) \frac{z^2 \bar{z}}{2} + \dots \quad (37)$$

Near the origin, on the manifold  $C_0$ , we have  $\dot{\mathbf{w}} = \mathbf{w}_z \dot{z} + \mathbf{w}_{\bar{z}} \dot{\bar{z}}$ . Using (32) and (34) to replace  $\mathbf{w}_z \dot{z}$  (and their conjugates, by their power series expansion) and equating with (36), we obtain the following operator equations:

$$(2j\omega_0 - \mathcal{A})\mathbf{w}_{20}(\theta) = H_{20}(\theta), \quad (38)$$

$$-\mathcal{A}\mathbf{w}_{11} = H_{11}(\theta), \quad (39)$$

$$-(2j\omega_0 + \mathcal{A})\mathbf{w}_{02}(\theta) = H_{02}(\theta). \quad (40)$$

We start by observing that

$$\mathbf{V}_t(\theta) = \mathbf{w}_{20}(\theta) \frac{z^2}{2} + \mathbf{w}_{02}(\theta) \frac{\bar{z}^2}{2} + \mathbf{w}_{11}(\theta) z\bar{z} + zq(\theta) + \bar{z}\bar{q}(\theta) + \dots$$

From the Hopf bifurcation analysis [2], we know that the coefficients of  $z^2$ ,  $\bar{z}^2$ ,  $z^2 \bar{z}$ , and  $z\bar{z}$  terms are used to approximate the system dynamics. Hence, we only retain these terms in the expansions. To that end, from (26), we evaluate the requisite terms. These are given by

$$\begin{aligned} v_{l,t}(-\tau_i) v_{i,t}(-\tau_i) &= (2\phi_l \phi_{i-1} e^{-j2\omega_0 \tau_i}) \frac{z^2}{2} + (2\bar{\phi}_l \bar{\phi}_{i-1} e^{j2\omega_0 \tau_i}) \frac{\bar{z}^2}{2} + (\phi_{i-1} \bar{\phi}_l + \phi_l \bar{\phi}_{i-1}) z\bar{z} \\ &\quad + \left( (w_{20l}(-\tau_i) \bar{\phi}_{i-1} + w_{20i}(-\tau_i) \bar{\phi}_l) e^{j\omega_0 \tau_i} \right) \frac{z^2 \bar{z}}{2} \\ &\quad + \left( (w_{11l}(-\tau_i) \phi_{i-1} + w_{11i}(-\tau_i) \phi_l) e^{-j\omega_0 \tau_i} \right) \frac{z^2 \bar{z}}{2}, \end{aligned} \quad (41)$$

$$v_{l,t}(-\tau_i) v_{n,t}(-\tau_i) v_{i,t}(-\tau_i) = (2\phi_l \phi_{i-1} \bar{\phi}_n e^{-j\omega_0 \tau_i}) \frac{z^2 \bar{z}}{2} + (2\phi_n (\phi_l \bar{\phi}_{i-1} + \phi_{i-1} \bar{\phi}_l) e^{-j\omega_0 \tau_i}) \frac{z^2 \bar{z}}{2}. \quad (42)$$

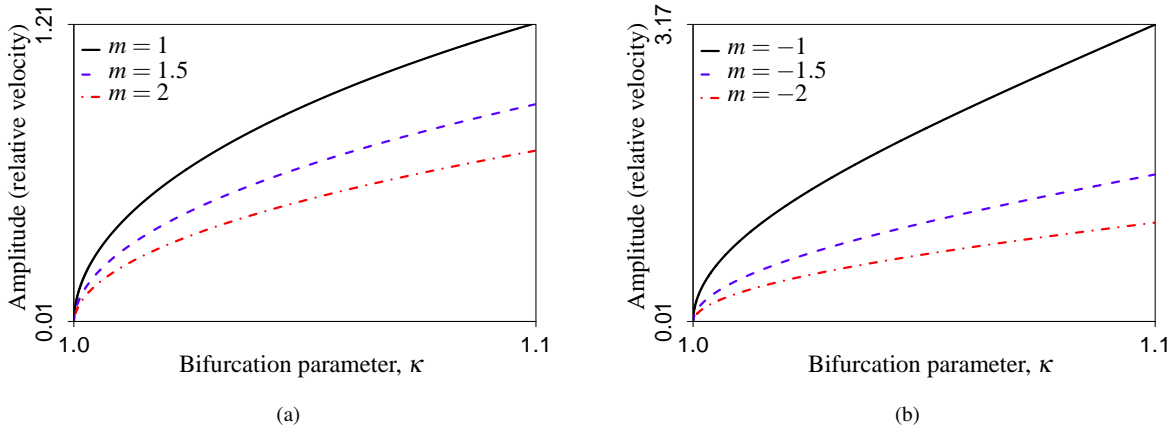


Fig. 3: The variation in the relative velocity amplitude of the limit cycle for the RCCFM, as  $\kappa$  is increased. (a) is for  $m > 0$ , while (b) is for  $m < 0$ . The amplitude of the emergent limit cycles increases as  $|m|$  increases. However, for 10% increase in  $\kappa$ , the variation in the amplitude for  $m > 0$  is smaller when compared to the case  $m < 0$ .

Substituting (41) and (42) in (26) yields the aggregation of the non-linear terms. For each  $i \in \{1, 2, \dots, N\}$ , it has the form:

$$\mathcal{F}_i = \mathcal{F}_{20i} \frac{z^2}{2} + \mathcal{F}_{02i} \frac{\bar{z}^2}{2} + \mathcal{F}_{11i} z \bar{z} + \mathcal{F}_{21i} \frac{z^2 \bar{z}}{2}, \quad (43)$$

where

$$\begin{aligned}
\mathcal{F}_{20i} &= \left( \frac{-4m\beta_{i-1}^* \phi_{i-2} e^{-j2\omega_0\tau_{i-1}}}{\dot{x}_0} \right) \sum_{l=1}^{i-1} \phi_{l-1} + \left( \frac{4m\beta_i^* \phi_{i-1} e^{-j2\omega_0\tau_i}}{\dot{x}_0} \right) \sum_{l=1}^i \phi_{l-1}, \\
\mathcal{F}_{02i} &= \left( \frac{-4m\beta_{i-1}^* \bar{\phi}_{i-2} e^{j2\omega_0\tau_{i-1}}}{\dot{x}_0} \right) \sum_{l=1}^{i-1} \bar{\phi}_{l-1} + \left( \frac{4m\beta_i^* \bar{\phi}_{i-1} e^{j2\omega_0\tau_i}}{\dot{x}_0} \right) \sum_{l=1}^i \bar{\phi}_{l-1}, \\
\mathcal{F}_{11i} &= \left( \frac{-2m\beta_{i-1}^*}{\dot{x}_0} \right) \sum_{l=1}^{i-1} (\phi_{l-1} \bar{\phi}_{i-2} + \phi_{i-2} \bar{\phi}_{l-1}) + \left( \frac{2m\beta_i^*}{\dot{x}_0} \right) \sum_{l=1}^i (\phi_{l-1} \bar{\phi}_{i-1} + \phi_{i-1} \bar{\phi}_{l-1}), \\
\mathcal{F}_{21i} &= \left( \frac{-2m\beta_{i-1}^* e^{j\omega_0\tau_{i-1}}}{\dot{x}_0} \right) \sum_{l=1}^{i-1} (w_{20l}(-\tau_{i-1}) \bar{\phi}_{i-2} + w_{20(i-1)}(-\tau_{i-1}) \bar{\phi}_{l-1}) \\
&\quad + \left( \frac{-4m\beta_{i-1}^* e^{-j\omega_0\tau_{i-1}}}{\dot{x}_0} \right) \sum_{l=1}^{i-1} (w_{11l}(-\tau_{i-1}) \phi_{i-2} + w_{20(i-1)}(-\tau_{i-1}) \phi_{l-1}) \\
&\quad + \left( \frac{2m\beta_i^* e^{j\omega_0\tau_i}}{\dot{x}_0} \right) \sum_{l=1}^i (w_{20l}(-\tau_i) \bar{\phi}_{i-1} + w_{20i}(-\tau_i) \bar{\phi}_{l-1}) \\
&\quad + \left( \frac{4m\beta_i^* e^{-j\omega_0\tau_i}}{\dot{x}_0} \right) \sum_{l=1}^i (w_{11l}(-\tau_i) \phi_{i-1} + w_{20i}(-\tau_i) \phi_{l-1}) \\
&\quad + \left( \frac{24m(m-1)\beta_{i-1}^* e^{-j\omega_0\tau_{i-1}}}{\dot{x}_0^2} \right) \sum_{l=1}^{i-1} \sum_{n=1}^{i-1} \phi_{l-1} \bar{\phi}_{n-1} \phi_{i-2} \\
&\quad + \left( \frac{24m(m-1)\beta_{i-1}^* e^{-j\omega_0\tau_{i-1}}}{\dot{x}_0^2} \right) \sum_{l=1}^{i-1} \sum_{n=1}^{i-1} \phi_{l-1} \phi_{n-1} \bar{\phi}_{i-2} \\
&\quad + \left( \frac{24m(m-1)\beta_{i-1}^* e^{-j\omega_0\tau_{i-1}}}{\dot{x}_0^2} \right) \sum_{l=1}^{i-1} \sum_{n=1}^{i-1} \bar{\phi}_{l-1} \phi_{n-1} \phi_{i-2} \\
&\quad + \left( \frac{-24m(m-1)\beta_i^* e^{-j\omega_0\tau_i}}{\dot{x}_0^2} \right) \sum_{l=1}^i \sum_{n=1}^i \phi_{l-1} \bar{\phi}_{n-1} \phi_{i-1} \\
&\quad + \left( \frac{-24m(m-1)\beta_i^* e^{-j\omega_0\tau_i}}{\dot{x}_0^2} \right) \sum_{l=1}^i \sum_{n=1}^i \phi_{l-1} \phi_{n-1} \bar{\phi}_{i-1} \\
&\quad + \left( \frac{-24m(m-1)\beta_i^* e^{-j\omega_0\tau_i}}{\dot{x}_0^2} \right) \sum_{l=1}^i \sum_{n=1}^i \bar{\phi}_{l-1} \phi_{n-1} \phi_i.
\end{aligned}$$

We represent the vector of non-linearities used in (33) as  $\mathcal{F}_0 = [\mathcal{F}_1 \ \mathcal{F}_2 \ \dots \ \mathcal{F}_N]^T$ . Next, we compute  $g$  using  $\mathcal{F}_0$  as

$$g(z, \bar{z}) = \bar{p}(0) \cdot \mathcal{F}_0 = \bar{B} \sum_{l=1}^N \bar{\psi}_{N-l} \mathcal{F}_l. \quad (44)$$

Substituting (43) in (44), and comparing with (35), we obtain

$$g_x = \bar{B} \sum_{l=1}^N \bar{\psi}_{N-l} \mathcal{F}_{xl}, \quad (45)$$

where  $x \in \{20, 02, 11, 21\}$ . Using (45), the corresponding coefficients can be computed. However, computing  $g_{21}$  requires  $\mathbf{w}_{20}(\theta)$  and  $\mathbf{w}_{11}(\theta)$ . Hence, we perform the requisite computation next. For  $\theta \in [-\tau, 0)$ ,  $H$  can be simplified as

$$\begin{aligned} H(z, \bar{z}, \theta) &= -\text{Real}(\bar{p}(0) \cdot \mathcal{F}_0 q(\theta)), \\ &= -\left(g_{20} \frac{z^2}{2} + g_{02} \frac{\bar{z}^2}{2} + g_{11} z \bar{z} + \dots\right) q(\theta) - \left(\bar{g}_{20} \frac{\bar{z}^2}{2} + \bar{g}_{02} \frac{z^2}{2} + \bar{g}_{11} z \bar{z} + \dots\right) \bar{q}(\theta), \end{aligned}$$

which, when compared with (37), yields

$$H_{20}(\theta) = -g_{20}q(\theta) - \bar{g}_{20}\bar{q}(\theta), \quad (46)$$

$$H_{11}(\theta) = -g_{11}q(\theta) - \bar{g}_{11}\bar{q}(\theta). \quad (47)$$

From (30), (38) and (39), we obtain the following ODEs:

$$\dot{\mathbf{w}}_{20}(\theta) = 2j\omega_0 \mathbf{w}_{20}(\theta) + g_{20}q(\theta) + \bar{g}_{02}\bar{q}(\theta), \quad (48)$$

$$\dot{\mathbf{w}}_{11}(\theta) = g_{11}q(\theta) + \bar{g}_{11}\bar{q}(\theta). \quad (49)$$

Solving (48) and (49), we obtain

$$\begin{aligned} \mathbf{w}_{20}(\theta) &= -\frac{g_{20}}{j\omega_0} q(0) e^{j\omega_0 \theta} - \frac{\bar{g}_{02}}{3j\omega_0} \bar{q}(0) e^{-j\omega_0 \theta} + \mathbf{e} e^{2j\omega_0 \theta}, \\ \mathbf{w}_{11}(\theta) &= \frac{g_{11}}{j\omega_0} q(0) e^{j\omega_0 \theta} - \frac{\bar{g}_{11}}{j\omega_0} \bar{q}(0) e^{-j\omega_0 \theta} + \mathbf{f}, \end{aligned}$$

for some vectors  $\mathbf{e}$  and  $\mathbf{f}$ , to be determined.

To that end, we begin by defining the following vector:  $\tilde{\mathcal{F}}_{20} \triangleq [\mathcal{F}_{201} \ \mathcal{F}_{202} \ \dots \ \mathcal{F}_{20N}]^T$ . Equating (46) and (38), and simplifying, yields the operator equation:  $2j\omega_0 \mathbf{e} - \mathcal{A}(\mathbf{e} e^{2j\omega_0 \theta}) = \tilde{\mathcal{F}}_{20}$ . On solving this, we obtain the following vector equality

$$2j\omega_0 \begin{bmatrix} \mathbf{e}_1 \\ \mathbf{e}_2 \\ \mathbf{e}_3 \\ \vdots \\ \mathbf{e}_N \end{bmatrix} - \begin{bmatrix} -\kappa\beta_1^* e^{-j\omega_0 \tau_1} \mathbf{e}_1 \\ \kappa\beta_1^* e^{-j\omega_0 \tau_1} \mathbf{e}_1 - \kappa\beta_2^* e^{-j\omega_0 \tau_2} \mathbf{e}_2 \\ \kappa\beta_2^* e^{-j\omega_0 \tau_2} \mathbf{e}_2 - \kappa\beta_3^* e^{-j\omega_0 \tau_3} \mathbf{e}_3 \\ \vdots \\ \kappa\beta_{N-1}^* e^{-j\omega_0 \tau_{N-1}} \mathbf{e}_{N-1} - \kappa\beta_N^* e^{-j\omega_0 \tau_N} \mathbf{e}_N \end{bmatrix} = \tilde{\mathcal{F}}_{20},$$

which, on simplifying, yields for  $i \in \{1, 2, \dots, N\}$ ,

$$\mathbf{e}_i = \frac{\mathcal{F}_{20i} + \kappa\beta_{i-1}^* e^{-j\omega_0 \tau_{i-1}} \mathbf{e}_{i-1}}{2j\omega_0 + \kappa\beta_i^* e^{-j\omega_0 \tau_i}},$$

where  $\mathbf{e}_0 = 0$  for notational brevity.

Next, equating (47) and (39), and simplifying, we obtain the operator equation  $\mathcal{A}\mathbf{f} = -\tilde{\mathcal{F}}_{11}$ , with  $\tilde{\mathcal{F}}_{11} \triangleq$

$[\mathcal{F}_{111} \ \mathcal{F}_{112} \ \cdots \ \mathcal{F}_{11N}]^T$ . On solving, we obtain:

$$\begin{bmatrix} -\kappa\beta_1^*\mathbf{f}_1 \\ \kappa\beta_1^*\mathbf{f}_1 - \kappa\beta_2^*\mathbf{f}_2 \\ \kappa\beta_2^*\mathbf{f}_2 - \kappa\beta_3^*\mathbf{f}_3 \\ \vdots \\ \kappa\beta_{N-1}^*\mathbf{f}_{N-1} - \kappa\beta_N^*\mathbf{f}_N \end{bmatrix} = -\tilde{\mathcal{F}}_{11},$$

which, on further simplification, yields

$$\mathbf{f}_i = \frac{\mathcal{F}_{11i} + \kappa\beta_{i-1}^*\mathbf{f}_{i-1}}{\kappa\beta_i^*},$$

for  $i \in \{1, 2, \dots, N\}$ , where  $\mathbf{f}_0 = 0$  for notational brevity.

Thus, we have obtained expressions for the vectors  $\mathbf{e}$  and  $\mathbf{f}$  required to compute  $\mathbf{w}_{20}(\theta)$  and  $\mathbf{w}_{11}(\theta)$ . This, in turn, facilitates the computation of  $g_{21}$ . We can now compute

$$c_1(0) = \frac{j}{2\omega_0} \left( g_{20}g_{11} - 2|g_{11}|^2 - \frac{1}{3}|g_{02}|^2 \right) + \frac{g_{21}}{2}, \quad \alpha'(0) = \text{Real} \left( \frac{d\lambda}{d\kappa} \right)_{\kappa=\kappa_{cr}},$$

$$\mu_2 = -\frac{\text{Real}(c_1(0))}{\alpha'(0)}, \quad \text{and } \beta_2 = 2\text{Real}(c_1(0)).$$

Here,  $c_1(0)$  is known as the Lyapunov coefficient and  $\beta_2$  is the Floquet exponent. These are useful since [2]

- (i) If  $\mu_2 > 0$ , then the bifurcation is *supercritical*, whereas if  $\mu_2 < 0$ , then the bifurcation is *subcritical*.
- (ii) If  $\beta_2 > 0$ , then the limit cycle is *asymptotically orbitally unstable*, whereas if  $\beta_2 < 0$ , then the limit cycle is *asymptotically orbitally stable*.

We present some numerical examples to gain some insights.

#### A. Numerical examples

We use the scientific computation software MATLAB to evaluate the required quantities. Throughout, we use SI units: distances will be in ‘meters,’ time in ‘seconds,’ velocity in ‘meters per second’ and  $\alpha$ ’s in ‘inverse second.’ For numerical computations, we use the following values.

- (i) This case summarises various scenarios considered in [8].  $N = 6, \dot{x}_0 = 5, \alpha_1 = 0.3, \alpha_2 = 0.5, \alpha_3 = 0.2, \alpha_4 = 0.4, \alpha_5 = 0.1, \alpha_6 = 0.6, \tau_1 = 1.2, \tau_2 = 1.7, \tau_3 = 2, \tau_4 = 2.7768, \tau_5 = 0.8$  and  $\tau_6 = 0.3$ . We vary the value of the non-linearity parameter  $m$ , and compute the corresponding values of  $\mu_2$  and  $\beta_2$ . These are as tabulated below.

SI Number	$m$	$\mu_2$	$\beta_2$
1	-2	60.8590	-0.3548
2	-1.5	16.7612	-0.2185
3	-1	3.2648	-0.0952
4	1	43.4211	-31.6383
5	1.5	439.6295	-716.2806
6	2	$2.4461 \times 10^3$	$-8.9116 \times 10^3$

For each of the above cases, the corresponding value implies that the 4<sup>th</sup> vehicle undergoes a *supercritical* Hopf bifurcation resulting in an asymptotically orbitally *stable* limit cycle.

- (ii)  $N = 5$ ,  $\dot{x}_0 = 35$ ,  $m = 1.5$ ,  $\alpha_i = 0.1 \forall i$ ,  $\tau_i = 0.0506 \forall i \neq 3$  and  $\tau_3 = 0.0759$ . The calculations yield  $\mu_2 = 4.4575 \times 10^{30}$ ,  $\beta_2 = -8.3628 \times 10^{31}$ . These values imply that the 3<sup>rd</sup> vehicle undergoes a *supercritical* Hopf bifurcation resulting in a *stable* limit cycle.
- (iii)  $N = 10$ ,  $\dot{x}_0 = 30$ ,  $m = 1.5$ ,  $\alpha_i = 0.06 \forall i$ ,  $\tau_i = 0.1062 \forall i \neq 5$  and  $\tau_5 = 0.1593$ . The calculations yield  $\mu_2 = 8.4507 \times 10^{31}$ ,  $\beta_2 = -7.5487 \times 10^{32}$ . These values imply that the 5<sup>th</sup> vehicle undergoes a *supercritical* Hopf bifurcation resulting in a *stable* limit cycle.
- (iv)  $N = 100$ ,  $\dot{x}_0 = 10$ ,  $m = 0.5$ ,  $\alpha_i = 0.05 \forall i$ ,  $\tau_i = 6.6231 \forall i \neq 50$  and  $\tau_{50} = 9.9346$ . The calculations yield  $\mu_2 = 8.7513 \times 10^{69}$ ,  $\beta_2 = -1.2537 \times 10^{69}$ . These values imply that the 50<sup>th</sup> vehicle undergoes a *supercritical* Hopf bifurcation resulting in a *stable* limit cycle.
- (v)  $N = 1$ ,  $\dot{x}_0 = 50$ ,  $m = 0.5$ ,  $\alpha_1 = 0.1$  and  $\tau_1 = 2.2214$ . The calculations yield  $\mu_2 = 0.0018$ ,  $\beta_2 = -0.0012$ . These values imply that the follower undergoes a *supercritical* Hopf bifurcation resulting in a *stable* limit cycle.

### B. Bifurcation diagrams

We next present bifurcation diagrams numerically constructed using DDE-BIFTOOL [16]. To begin with, we feed the requisite delay differential equations, with their first-order derivatives, as the input to DDE-BIFTOOL. Then, we fix  $\kappa = 1$ , initialize the model parameters with suitable values and set a range for the parameter of interest to vary in. DDE-BIFTOOL then varies this parameter and finds the critical value at which the system undergoes a Hopf bifurcation. We then increase the value of the non-dimensional parameter and record the amplitude of the resulting limit cycle pertaining to the relative velocity to obtain the bifurcation diagram. In the following, time units are expressed in ‘seconds,’ velocity in ‘meters per second’ and  $\alpha$ ’s in ‘inverse second.’

We initialise the parameters with the following values.  $N = 6$ ,  $\alpha_1 = 0.3$ ,  $\alpha_2 = 0.5$ ,  $\alpha_3 = 0.2$ ,  $\alpha_4 = 0.4$ ,  $\alpha_5 = 0.1$ ,  $\alpha_6 = 0.6$ ,  $\tau_1 = 1.2$ ,  $\tau_2 = 1.7$ ,  $\tau_3 = 2$ ,  $\tau_4 = 2.7768$ ,  $\tau_5 = 0.8$  and  $\tau_6 = 0.3$ . The leader’s equilibrium velocity is set to 5, and we consider  $m = \pm 1, \pm 1.5$ , and  $\pm 2$ .

Figs 3a and 3b correspond to the bifurcation diagrams for the RCCFM for positive and negative values of the non-linearity parameter  $m$  respectively. As seen from these figures, the amplitude of the emergent limit cycle decreases with increase in  $|m|$ , as  $\kappa$  is varied from 1 to 1.1. Moreover, for a given value of  $\kappa$ , the amplitude of the emergent limit cycles for positive values of  $m$  is lower than when  $m$  is negative. This observation suggests that it would be better to use  $m = 2$  for the design of a control algorithm for self-driven vehicles.

## IX. SIMULATIONS

Thus far, we have analysed the RCCFM for no-delay, small-delay and arbitrary-delay regimes. We also characterised the stable region for the RCCFM, and studied two of its important aspects – non-oscillatory convergence and

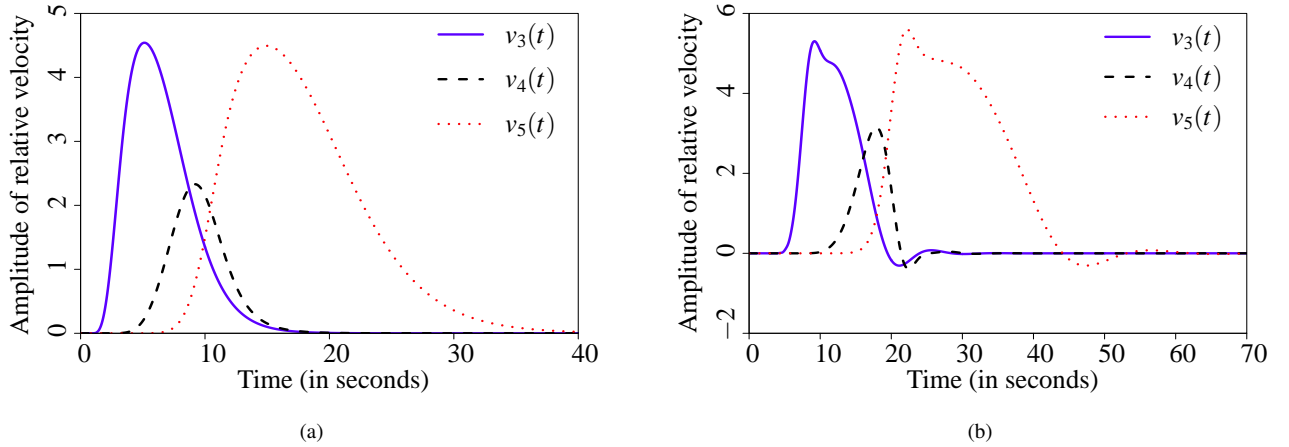


Fig. 4: Figure portraying non-oscillatory and oscillatory convergences in the RCCFM. (a) shows the non-oscillatory convergence of the solution for  $\tau < \tau^*$ , whereas (b) shows the solutions oscillation about the equilibrium before converging, for  $\tau > \tau^*$ .

the rate of convergence. In the previous section, we characterised the type of Hopf bifurcation and the asymptotic orbital stability of the limit cycles that emerge when the stability conditions are marginally violated.

In this section, we present the simulation results of the RCCFM, that serve to corroborate our analytical findings. We make use of the scientific computation software MATLAB to implement a discrete version of system (3), thus simulating the RCCFM. We use  $T_s = 0.01$  s as the update time. Throughout, we use SI units.

We initialise the parameters with the following values, as in [8].  $N = 6$ ,  $\alpha_1 = 0.3$ ,  $\alpha_2 = 0.5$ ,  $\alpha_3 = 0.2$ ,  $\alpha_4 = 0.4$ ,  $\alpha_5 = 0.1$ ,  $\alpha_6 = 0.6$ ,  $\tau_1 = 1.2$ ,  $\tau_2 = 1.7$ ,  $\tau_3 = 2$ ,  $\tau_4 = 2.7768$ ,  $\tau_5 = 0.8$  and  $\tau_6 = 0.3$ . The leader's velocity profile is considered to be  $5(1 - e^{-10t})$ , thus ensuring an equilibrium velocity of 5. Further, we fix  $m = 0.5$ . Fig. 5 shows the emergence of limit cycles, as predicted by the transversality condition of the Hopf spectrum (19).

Next, we validate that the RCCFM does indeed exhibit non-oscillatory convergence to the all-zero equilibrium, as predicted by (23). We also compare the rate of convergence when the reaction delay satisfies  $\tau < \tau^*$  and  $\tau > \tau^*$ , as discussed in Section VII. For illustration purposes, we use the following parameter values.  $N = 6$ ,  $\alpha_1 = 0.3$ ,  $\alpha_2 = 0.5$ ,  $\alpha_3 = 0.2$ ,  $\alpha_4 = 0.4$ ,  $\alpha_5 = 0.1$  and  $\alpha_6 = 0.6$ . We let  $m = 0.5$ , and the leader's velocity profile is considered to be  $5(1 - e^{-10t})$ , thus ensuring an equilibrium velocity of 5. For each vehicle, the corresponding reaction delay is computed as  $\tau_1 = 1/(2e\beta^*)$  and  $\tau_2 = 2/(e\beta^*)$ . Figs 4a and 4b portray the non-oscillatory and the oscillatory behaviour of the solutions, respectively. Notice that  $\tau_1 = \tau^*/2$  and  $\tau_2 = 2\tau^*$ , which is not in the vicinity of  $\tau^*$  for the fourth vehicle (the vehicle with  $\alpha = 0.4$ , as considered while plotting Fig. 2), as seen from Fig. 4. Hence, the corresponding solution (marked by dotted line) shown in Fig. 4a equilibrates much faster than its counterpart portrayed in Fig. 4b.

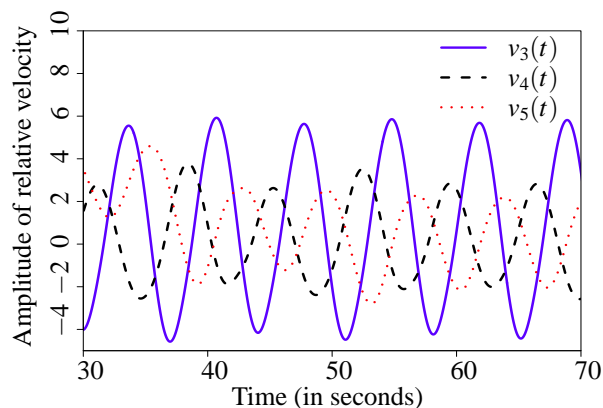


Fig. 5: Figure showing the emergence of limit cycles in simulations, thus validating the RCCFM.

## X. CONCLUDING REMARKS

In this paper, we highlighted the importance of delayed feedback in determining the qualitative dynamical properties of a platoon of vehicles driving on a straight road. Specifically, we analysed the Reduced Classical Car-Following Model (RCCFM) in three regimes – no delay, small delay and arbitrary delay. Control-theoretic analyses helped us derive conditions for its local stability. In particular, the analysis for small-delay regime yielded a sufficient condition for the local stability of the RCCFM, whereas we obtained the necessary and sufficient condition for the local stability of the RCCFM in the arbitrary-delay regime.

We then proved that the RCCFM undergoes a loss of stability via a Hopf bifurcation. Mathematically, this result proves the emergence of limit cycles, which physically manifests as a back-propagating congestion wave. Even though the parameters are not strictly controllable in the case of human drivers, our work enhances the phenomenological insights into ‘phantom jams.’ Our analyses made use of an exogenous, non-dimensional parameter that served to handle the complex relation which could exist among the various model parameters.

We then derived the necessary and sufficient condition for non-oscillatory convergence of the RCCFM. Designing control algorithms that conform to this condition ensures that jerky vehicular motions are avoided, thus guaranteeing smooth traffic flow and improving ride quality. Next, we characterised the rate of convergence of the RCCFM, and highlighted the trade-off between non-oscillatory convergence and the rate of convergence.

Finally, we characterised the type of Hopf bifurcation and the asymptotic orbital stability of the limit cycles, which emerge when the stability conditions are just violated, using Poincaré normal forms and the center manifold theory. The analyses were then complemented by stability charts, numerically constructed bifurcation diagrams and MATLAB simulations. These serve to highlight the impact of various model parameters on system stability as well as the relative velocity amplitude of the bifurcating limit cycles.

### *Avenues for further research*

There are numerous avenues that merit further investigation. In the general context of car-following models, several other models including the Optimal Velocity Model (OVM) [18] and Modified Optimal Velocity Model (MOVM) [8] are known to lose local stability via a Hopf bifurcation. However, several other properties of these models, such as the rate of convergence, non-oscillatory convergence and robustness to parameter variations, are not fully understood.

In the context of the Classical Car-Following Model, in this work, we have considered the special case corresponding to  $l = 0$ , as mentioned in Section II-C. The case  $l \neq 0$  remains to be investigated for more exotic flavours of bifurcation phenomena. Further, we have derived conditions for pairwise stability of vehicles in this work. However, string stability of a platoon of vehicles running the RCCFM remains to be studied.

From a practical standpoint, the parameters of the RCCFM may vary, for varied reasons. Hence, it becomes imperative that the longitudinal control algorithm be robust to such parameter variations, and to unmodeled vehicular dynamics.

### ACKNOWLEDGEMENTS

This work is undertaken as a part of an Information Technology Research Academy (ITRA), Media Lab Asia, project titled “De-congesting India’s transportation networks”. The authors are also thankful to Debayani Ghosh and Sreelakshmi Manjunath for many helpful discussions.

### REFERENCES

- [1] A. Kesting and M. Treiber, “How reaction time, update time, and adaptation time influence the stability of traffic flow”, *Computer-Aided Civil and Infrastructure Engineering*, vol. 23, pp. 125-137, 2008.
- [2] B.D. Hassard, N.D. Kazarinoff and Y.-H. Wan, “Theory and Applications of Hopf Bifurcation.”, *Cambridge University Press*, 1981.
- [3] D.C. Gazis, R. Herman and R.W. Rothery, “Nonlinear follow-the-leader models of traffic flow”, *Operations Research*, vol. 9, pp. 545-567, 1961.
- [4] D. Chowdhury, L. Santen and A. Schadschneider, “Statistical physics of vehicular traffic and some related systems”, *Physical Reports*, vol. 329, pp. 199-329, 2000.
- [5] D. Helbing, “Traffic and related self-driven many-particle systems”, *Reviews of Modern Physics*, vol. 73, pp. 1067-1141, 2001.
- [6] E.A. Unwin and L. Duckstein, “Stability of reciprocal-spacing type car-following models”, *Transportation Science*, vol. 1, pp. 95-108, 1967.
- [7] F. Brauer, “Decay rates for solutions of a class of differential-difference equations”, *SIAM Journal on Mathematical Analysis*, vol. 10, pp. 783-788, 1979.
- [8] G.K. Kamath, K. Jagannathan and G. Raina, “Car-following models with delayed feedback: local stability and Hopf bifurcation”, in *Proceedings of the 53<sup>rd</sup> Annual Allerton Conference on Communication, Control and Computing*, 2015.
- [9] G. Orosz and G. Stépán, “Subcritical Hopf bifurcations in a car-following model with reaction-time delay”, *Proceedings of the Royal Society A*, vol. 642, pp. 2643-2670, 2006.
- [10] G. Raina, “Local bifurcation analysis of some dual congestion control algorithms”, *IEEE Transactions on Automatic Control*, vol. 50, pp. 1135-1146, 2005.
- [11] G. Strang, “Linear Algebra and Its Applications”, *Cengage Learning*, Fourth Edition, 2006.
- [12] I. Györi and G. Ladas, “Oscillation Theory of Delay Differential Equations With Applications”, *Clarendon Press*, 1991.
- [13] I.N. Herstein, “Topics in Algebra”, *John Wiley & Sons*, 1975.

- [14] J.K. Hale and S.M.V. Lunel, "Introduction to Functional Differential Equations", *Springer-Verlag*, 2011.
- [15] K.C. Dey, L. Yan, X. Wang, Y. Wang, H. Shen, M. Chowdhury, L. Yu, C. Qiu and V. Soundararaj, "A review of communication, driver characteristics, and controls aspects of cooperative adaptive cruise control (CACC)", *IEEE Transactions on Intelligent Transportation Systems*, vol. 17, pp. 491-509, 2016.
- [16] K. Engelborghs, T. Luzyanina and D. Roose, "Numerical bifurcation analysis of delay differential equations DDE-BIFTOOL", *ACM Transactions on Mathematical Software (TOMS)*, vol. 28, pp. 1-21, 2002.
- [17] K.J. Åström and R.M. Murray, "Feedback Systems: An Introduction for Scientists and Engineers", *Princeton University Press*, 2008.
- [18] M. Bando, K. Hasebe, K. Nakanishi and A. Nakayama, "Analysis of optimal velocity model with explicit delay", *Physical Review E*, vol. 58, pp. 5429-5435, 1998.
- [19] R.E. Chandler, R. Herman and E.W. Montroll, "Traffic dynamics: studies in car following", *Operations Research*, vol. 6, pp. 165-184, 1958.
- [20] R.E. Wilson and J.A. Ward, "Car-following models: fifty years of linear stability analysis - a mathematical perspective", *Transportation Planning and Technology*, vol. 34, pp. 3-18, 2011.
- [21] R. Herman, E.W. Montroll, R.B. Potts and R.W. Rothery, "Traffic dynamics: analysis of stability in car following", *Operations Research*, vol. 7, pp. 86-106, 1959.
- [22] R. Rajamani and C. Zhu, "Semi-autonomous adaptive cruise control systems", *IEEE Transactions on Vehicular Technology*, vol. 51, pp. 1186-1192, 2002.
- [23] R. Rajamani, "Vehicle Dynamics and Control", *Springer*, Second Edition, 2012.
- [24] R. Sipahi and S.I. Niculescu, "Analytical stability study of a deterministic car following model under multiple delay interactions", in *Proceedings of Mechanical and Industrial Engineering Faculty Publications*, 2006.
- [25] R.U. Chavan, M. Belur, D. Chakraborty and D. Manjunath, "On the stability and formations in ad hoc multilane vehicular traffic", in *Proceedings of the 7<sup>th</sup> International Conference on Communication Systems and Networks (COMSNETS)*, 2015.
- [26] S. Deb and R. Srikant, "Global stability of congestion controllers for the Internet", *IEEE Transactions on Automatic Control*, vol. 48, pp. 1055-1060, 2003.
- [27] S. Greengard, "Smart transportation networks drive gains", *Communications of the ACM*, vol. 58, pp. 25-27, 2015.
- [28] T.H. Summers, C. Yu, S. Dasgupta and B.D.O. Anderson, "Control of minimally persistent leader-remote-follower and coleader formations in the plane", *IEEE Transactions on Automatic Control*, vol. 56, pp. 2778-2792, 2011.
- [29] W. Rudin, "Real & Complex Analysis", *Tata McGraw Hill Publications*, Third Edition, 1987.
- [30] X. Zhang and D.F. Jarrett, "Stability analysis of the classical car-following model", *Transportation Research Part B*, vol. 31, pp. 441-462, 1997.
- [31] Z. Qu, J. Wang and R.A. Hull, "Cooperative control of dynamical systems with application to autonomous vehicles", *IEEE Transactions on Automatic Control*, vol. 53, pp. 894-911, 2008.